Anomalous *k*-dependent spin splitting in wurtzite $Al_xGa_{1-x}N/GaN$ heterostructures

Ikai Lo,* M. H. Gau, J. K. Tsai, Y. L. Chen, Z. J. Chang, W. T. Wang, and J. C. Chiang
Department of Physics, Center for Nanoscience and Nanotechnology, National Sun Yat-Sen University, Kaohsiung, Taiwan, Republic of China

T. Aggerstam and S. Lourdudoss
KTH Royal Institute of Technology, Electrum 229, SE-164 40 Kista, Sweden

(Received 19 January 2007; revised manuscript received 27 February 2007; published 6 June 2007)

We have observed the *k*-dependent spin splitting in wurtzite $Al_xGa_{1-x}N/GaN$ heterostructures. An anomalous beating pattern was observed in Shubnikov–de Haas measurements due to the interference of Rashba and Dresselhaus spin-orbit interactions. The dominant mechanism for the *k*-dependent spin splitting at high values of *k* is attributed to Dresselhaus term which is enhanced by the Δ_{C1}-Δ_{C3} coupling of wurtzite band folding effect. The interference of Rashba and Dresselhaus effects in the $Al_xGa_{1-x}N/GaN$ heterostructure provides a potential candidate for the gate-controlled spin-polarized spintronic devices.

DOI: 10.1103/PhysRevB.75.245307 PACS number(s): 72.25.Dc, 71.70.Ej

I. INTRODUCTION

Spin-orbit interaction is the key issue of spin dynamics in semiconductor spintronics.[1,2] It originates from the relativistic theory of Dirac's equation to assure symmetry in the wave equation with respect to space and time derivatives.[3] In the atomic case, it is formulated as $\boldsymbol{H}_{SO}=(ge\hbar/4m_0^2c^2)\vec{\sigma}\cdot(\vec{p}\times\nabla V)$ for the electron spin interacting with the electric field $(\boldsymbol{E}=-\nabla V)$ produced by the nucleus with respect to its orbital motion, where $\vec{\sigma}$ is the Pauli matrix, g is the g factor of free electron, and $\vec{p}$ is the momentum of electron. In III-V semiconductor heterostructures, there are two effects contributing to the spin-orbit interaction: (i) the structure inversion asymmetry (SIA) of electrostatic confinement potential at heterointerface, i.e., $\nabla V=\hat{z}(dV/dz)$ (known as the Rashba effect), and (ii) the bulk inversion asymmetry (BIA) of the lattice structure in which the coupling between the s wave of atom A (e.g., s_A) and the p wave of atom B (e.g., p_B) is not equal to that between the p wave of atom A (e.g., p_A) and the s wave of atom B (e.g., s_B), i.e., $U(s_A,p_B)-U(p_A,s_B)\neq 0$ (named the Dresselhaus effect). In *zinc-blende* structure, the 2D Hamiltonian for the SIA term can be written as $\boldsymbol{H}_R(\boldsymbol{k})=\alpha(\sigma_x k_y-\sigma_y k_x)$, where the Rashba coefficient α is proportional to the electric field built at heterointerface, $\alpha=\alpha_0 e\boldsymbol{E}$,[4] while for BIA term, it becomes $\boldsymbol{H}_D(\boldsymbol{k})=\gamma[\langle k_z^2\rangle(\sigma_y k_y-\sigma_x k_x)+(\sigma_x k_x k_y^2-\sigma_y k_y k_x^2)]$, where the z axis is the growth direction and the Dresselhaus constant (γ) is proportional to the strength of the BIA spin-orbit interaction.[5–8] If we only consider the linear-$\boldsymbol{k}$ terms, then $\boldsymbol{H}_D$ and $\boldsymbol{H}_R$ are coupled by each other, leading to an anisotropic linear-$\boldsymbol{k}$-dependent interference: $\boldsymbol{H}_{SO}(\boldsymbol{k})=\boldsymbol{H}_R(\boldsymbol{k})+\boldsymbol{H}_D(\boldsymbol{k})=\alpha(\sigma_x k_y-\sigma_y k_x)+\beta(\sigma_x k_x-\sigma_y k_y)$, where $\beta=-\gamma\langle k_z^2\rangle=-\gamma(\pi/d)^2$ and d is the size of quantum confinement.[9,10] The degree of specular asymmetry of two-dimensional electron gas (2DEG) at heterointerface can be controlled by a gate voltage, and thus the relative contributions of the two effects are tunable.[10–13] The spin splitting becomes anisotropic when the two contributions are comparable, giving an anomalous beating pattern in magneto-oscillations, e.g., Shubnikov–de Haas (SdH) oscillations. The suppression of beating pattern due to the interference of Rashba and Dresselhaus effects was individually proposed by Tarasenko *et al.*[11] and by Ting *et al.*[10] The interplay between Rashba and Dresselhaus effects activates a crucial impact in spin dynamics,[9] and a large Dresselhaus term provides significant enhancement for polarization efficiency in spintronic application.[10] Recently, the candidate material for a large Dresselhaus term is focused on III-nitride compounds due to their inherent property of bulk structure inversion asymmetry in the z direction.[14]

II. SPIN-ORBIT INTERACTION IN WURTZITE GaN

In wurtize $Al_xGa_{1-x}N/GaN$, the effective spin-splitting energy $\Delta E_{SO}^*(k)$ measured by SdH oscillations is widely spread from 0 to 11 meV,[14–18] Table I. In theory, the calculated Rashba spin splitting by a four-band model $(\Delta E_R<1$ meV) is much smaller than the experimental values.[19] On the other hand, the Dresselhaus effect was

TABLE I. The effective spin-splitting energy versus Al composition.

x	Si-doped at AlGaN (10^{18} cm^{-3})	mobility (10^3 cm^2/V s)	n_1 (10^{12} cm^{-2})	ΔE_{SO}^* (meV)
0.11[a]	Undoped	9.15	5.40	2.5
0.15[b]	Undoped	7.39	2.4–4.2	4.4–4.8
0.15[c]	5.0	9.54	7.12–7.57	2.7–3.6
0.22[d]	Undoped	8.10	8.68–9.39	0–10.38
0.25[e,f]	0.17	6.10	8.16–8.39	4.36–11.2
0.30[b]	Undoped	6.82	8.0	0
0.31[f]	3.0	4.0	10.30	5.91

[a]Reference 18.
[b]Reference 17.
[c]Reference 15.
[d]This work.
[e]Reference 14.
[f]Reference 16.

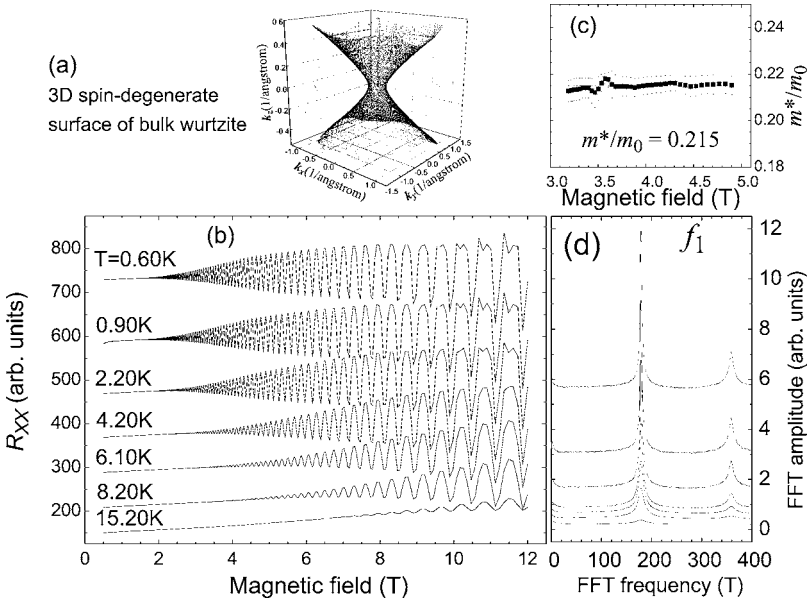

FIG. 1. (a) Schematic diagram of spin-degenerate sandglass cone for a bulk wurtzite structure, which obeys the degenerate equation $[\alpha_{wz}-\gamma_{wz}(bk_z^2-k_\parallel^2)]=0$. (b) The temperature dependent SdH measurements before illumination. (c) The effective mass determined from (b) versus magnetic field. (d) The FFT spectra of the temperature-dependent SdH measurements.

evaluated in wurtzite lattice with intrinsic bulk inversion asymmetry by Lew Yan Voon *et al.*[20] It was pointed out that the linear-$\boldsymbol{k}$ term can also arise from the weak s-p_z mixing of conduction band at $\boldsymbol{k}=0$ due to the second Ga-N neighbor interaction.[21] However, the Dresselhaus spin-splitting energy calculated by the four-band model is very small (e.g., $\Delta E_D < 0.5$ and 0.05 meV for CdS and ZnO, respectively).[20] Therefore, the Rashba and Dresselhaus effects, which consider the spin-orbit interaction between conduction and valence bands (the four-band model), are not enough to account for the large spin splitting observed in $Al_xGa_{1-x}N/GaN$. Recently, we proposed a model of Δ_{C1}-Δ_{C3} coupling to interpret the large spin splitting, which is caused by a band folding effect due to the different sizes of unit cells in the hexagonal direction between zinc-blende and wurtzite lattices.[22] Therefore, we can extend the Rashba term to include the intrinsic wurtzite structure inversion asymmetry (WSIA) effect,[4,21] which leads to a linear-$\boldsymbol{k}$ term, $\boldsymbol{H}_R(\boldsymbol{k})=\alpha_{wz}(\sigma_x k_y-\sigma_y k_x)$, with $\alpha_{\mathrm{wz}}=\alpha_0 e\boldsymbol{E}+\boldsymbol{C}_{\mathrm{WSIA}}$. Here, for convenient reasons, we used the Rashba coefficient (α_{wz}) to represent the WSIA constant ($\boldsymbol{C}_{\mathrm{WSIA}}$) term, as well as the term induced by the electric field at heterointerface ($\boldsymbol{E}$). Therefore, the WSIA constant ($\boldsymbol{C}_{\mathrm{WSIA}}$) represents the linear-$\boldsymbol{k}$ term of net effect due to the WSIA, including the linear-$\boldsymbol{k}$ term induced by the weak s-p_z mixing of conduction band due to the second Ga-N neighbor interactions[21] and the linear-$\boldsymbol{k}$ term caused by crystal field and strain.[20] In the meanwhile, the Dresselhaus term becomes $\boldsymbol{H}_D(\boldsymbol{k})=\gamma_{wz}(k_\parallel^2-bk_z^2)(\sigma_x k_y-\sigma_y k_x)$, where $b=4$ for an ideal wurtzite. Both $\boldsymbol{H}_R$ and $\boldsymbol{H}_D$ are proportional to $(\sigma_x k_y-\sigma_y k_x)$. This isotropic behavior was recently demonstrated to evaluate the Rashba term in GaN/AlGaN.[23] However, the Rashba term itself has only a spin degeneracy at the Γ point ($\boldsymbol{k}=0$), implying that the observation of spin-degenerate states other than the Γ point evidences the presence of the Dresselhaus term. The Hamiltonian for the $\boldsymbol{H}_R$ and $\boldsymbol{H}_D$ interference becomes isotropic: $\boldsymbol{H}_{\mathrm{SO}}(\boldsymbol{k})=[\alpha_{wz}-\gamma_{wz}(bk_z^2-k_\parallel^2)]\times(\sigma_x k_y-\sigma_y k_x)$. The suppression of the beating pattern due to the interference of $\boldsymbol{H}_D$ and $\boldsymbol{H}_R$ turns into a spin-degenerate sandglass cone with a degenerate equation: $[\alpha_{wz}-\gamma_{wz}(bk_z^2-k_\parallel^2)]=0$. The schematic spin-degenerate sandglass surface for a bulk wurtizte structure is plotted with $\gamma_{wz}=4.735$ [eV/$(\pi/c)^3$] and $\alpha_{wz}=-0.047\,35$ [eV/(π/c)] in Fig. 1(a). Besides, in $Al_xGa_{1-x}N/GaN$ the piezoelectric field built at heterointerface[24] can enhance the Rashba effect, as well. Therefore, the mechanism of spin splitting consists of four parts: Rashba (α_{wz}) term, Dresselhaus (β_{wz}) term, piezoelectric field, and Δ_{C1}-Δ_{C3} coupling. The heterointerface of $Al_xGa_{1-x}N/GaN$ plays a role to offer an x-dependent conduction band offset and a piezoelectric field. Consequently, the gate-controlled spin-splitting 2DEG at heterointerface provides a potential candidate for the application of spintronic devices.

III. SHUBNIKOV–de HAAS MEASUREMENT

The $Al_xGa_{1-x}N/GaN$ samples were grown by metal-organic chemical-vapor deposition on a c-plane sapphire with ferrocene as an iron doping source. Above the sapphire substrate, the sample consists of a 100-nm-thick GaN buffer layer, an 800-nm-thick Fe-doped GaN layer, an unintentionally doped 1.6-μm-thick GaN layer, and an unintentionally doped 25-nm-thick $Al_xGa_{1-x}N$ barrier layer on the top. The Fe-doped impurities are used to form deep-level electron traps to capture the n-type carriers as an insulating buffer (the activation energy is 0.5 eV).[25] A Hall-bar-shaped 2×6 mm^2 sample ($x=0.22$) with indium Ohmic contacts was annealed at 350 °C for 5 min under N_2 forming gas. The persistent photoconductivity (PPC) effect was provided by illuminating the sample at $T\sim0.38$ K for different time periods using a blue-light-emitting diode of 472 nm wavelength. Before illumination, the carrier concentration is 9.1×10^{12} cm^{-2} and the mobility is 8.1×10^3 cm^2/V s (determined from Hall measurement at $T\sim0.38$ K). After an extensive illumination, the carrier concentration increases by 14% to 10.4×10^{12} cm^{-2}, but the mobility decreases to 6.3×10^3 cm^2/V s. The increased carriers were mostly trans-

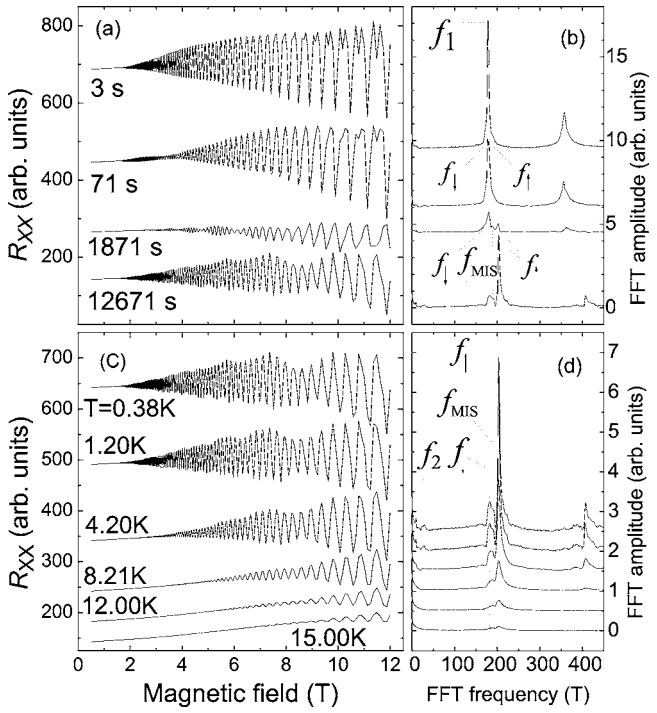

FIG. 2. (a) The SdH measurements for different illumination times at $T=0.38$ K and (b) their FFT spectra. (c) The temperature-dependent SdH measurements after the 12671 s illumination and (d) their FFT spectra.

ferred from the deep-level electron traps located at the remote Fe-doped GaN layer.[26] We performed the SdH measurement on the sample for the magnetic field (B) from 0.5 to 12 T. Because the oscillation part of magnetoresistance (R_{XX}) is a cosine function against $1/B$, the SdH data (2048 points) were taken with equal spacing of $1/B$ for the purpose of fast Fourier transformation (FFT). The resolution of the SdH frequency in the FFT spectrum is equal to 0.26 T, which can detect the change of 0.13×10^{11} cm^{-2} in the 2D carrier concentration. The SdH measurements and their FFT spectra at different temperatures before illumination are shown in Figs. 1(b) and 1(d). A single oscillation is detected at frequency $f_1=179.27$ T, giving the carrier concentration of first subband $n_1=2f_1e/h=8.68\times10^{12}$ cm^{-2}, and a Zeeman splitting is observed at high fields (e.g., $B>10$ T) for temperatures lower than 2.20 K.[27] Since the first subband carrier concentration is less than the Hall carrier concentration, the excess carriers may reside in the second subband. Because of the greater mobility, only the SdH oscillation of the first subband is detected. It is confirmed by the measured effective mass extracted from the temperature dependence of SdH amplitudes at the fields of peak positions [Fig. 1(c)]. The average value of the mass ($m^*/m_0=0.215\pm0.003$) is equal to the first subband effective mass.[16]

Figure 2 shows the SdH measurements and their FFT spectra after the PPC effect for different illumination times. The spin splitting of the first subband (i.e., $f_\uparrow$ and $f_\downarrow$) appears after 71 s illumination, and the peaks separate farther for a longer illumination until saturation [Fig. 2(b)]. The amplitude of the spin-down oscillation ($f_\downarrow$) decreases with the illumination time, but that of the spin-up oscillation ($f_\uparrow$) increases, relatively. Zeeman splitting also appears at high fields for 3 and 71 s illuminations. Zeeman splitting has been observed by Cho *et al.*[27] and analyzed in the presence of Rashba and Dresselhaus effects by de Andrada e Silva *et al.*[28] It was shown that the Zeeman splitting can be detected at high fields as the Zeeman energy is greater than the energy of the spin-orbit interaction. The effective g factor is about 2 for GaN,[27] and hence, the Zeeman splitting for $B>10$ T ($\Delta E_Z>0.58$ meV) is greater than the effective spin-splitting energy (ΔE_{SO}^*) in the first two measurements (3 and 71 s). Since Zeeman splitting is linearly dependent on B ($\Delta E_Z=g^*\mu_B B$), it produces only a phase constant in the SdH oscillation and will not change the frequency for large Landau levels like our case. As a result, Zeeman splitting enhances the amplitude of the second harmonic peak in the FFT spectrum [see the peak at $2f_1$ frequency in Fig. 1(b)]. In Fig. 2(b), a third peak (f_{MIS}) is growing between the two spin-splitting peaks in the longer illuminations. A three-peak SdH pattern was reported by Tsubaki *et al.*[15] and by Averkiev *et al.*[29] The former attributed the third peak to a magnetointersubband scattering (MIS) component, and the latter ascribed it to the third harmonics of the interference of Rashba and Dresselhaus terms. The MIS component is a second-order resonant scattering oscillation between the first (f_1) and second (f_2) subbands with a frequency $f_{MIS}=f_1$-f_2, and its amplitude does not contain the temperature damping factor. Without the temperature damping factor, the MIS component is less sensitive to the change of temperature. We checked the SdH oscillations at different temperatures after 12671 s illumination and showed them in Figs. 2(c) and 2(d). It is evident that there is no change in the frequencies when the temperature increases. The amplitude of the f_{MIS} peak has less sensitivity to temperature, but the temperature sensitivity of $f_\uparrow$ and $f_\downarrow$ peaks is consistent with that of f_1 peak in Fig. 1(d). Besides, the value of the f_{MIS} frequency is approximately equal to the difference of $f_\uparrow$ and f_2 frequencies. Therefore, we conclude that the peak of f_{MIS} is due to the MIS component between the $f_\uparrow$ and f_2 oscillations. In addition, Thillosen *et al.* mentioned another possibility of beating effect in SdH oscillations: the inhomogeneities in the AlGaN barrier, which will produce a weak antilocalization effect.[17] Because both weak antilocalization and weak localization effects[30] are induced by the inhomogeneities in a 2DEG due to the electron-electron interaction, they will generate a negative magnetoresistance at low magnetic field, i.e., negative $\Delta R_{XX}(B)=R_{XX}(B)-R_{XX}(0)$. Because of the absence of negative magnetoresistance in Fig. 2, we also eliminated the possibility of beating pattern induced by inhomogeneities. In order to evaluate these peaks more precisely against the illumination time, we repeated the SdH measurements after warming up the sample at room temperature for a couple of days. Figure 3 shows the precise measurements at $T\sim0.38$ K and their FFT spectra. The single SdH oscillation (f_1 peak) is detected for the illumination time less than 193 s, and it splits apparently after 313 s illumination [Fig. 3(b)]. The two spin-splitting peaks separate farther by longer illuminations. The amplitude of the $f_\downarrow$ peak decreases, but that of the $f_\uparrow$ peak increases with the illumination time, as observed in Fig. 2. In the last two spectra, it is clearly shown

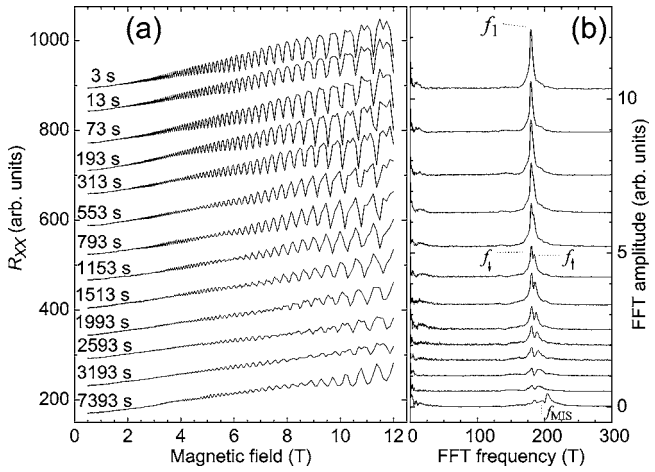

FIG. 3. (a) The SdH measurements against the illumination time at $T=0.38$ K and (b) their FFT spectra.

that the f_{MIS} peak is split away from the $f_\uparrow$ peak. The SdH frequencies versus total illumination time are plotted in Fig. 4(a); the open circles indicate the f_1 frequency before splitting, and $f_\uparrow$ (soild circles) and $f_\downarrow$ (solid squares) are the frequencies of spin-up and spin-down first subbands. We calculated the carrier concentrations for the two spin subbands from the SdH frequencies and plotted them against the first subband carrier concentration (i.e., $n_1=n_\uparrow+n_\downarrow$) in Fig. 4(b), where $n_i=f_i e/h$. The factor of 2 is removed due to the lift of spin degeneracy. The effective spin-splitting energy was calculated from the carrier concentrations of spin subbands, $\Delta E^*_{\mathrm{SO}}=2\pi\hbar^2(n_\uparrow-n_\downarrow)/m^*$, and plotted against the mean Fermi wave vector, $k_F^{\parallel}=(2\pi n_1)^{1/2}$, in Fig. 4(c). We obtained the k-dependent ΔE^*_{SO} and extrapolated it to zero at $k_F^{\parallel}=7.37\times10^8$ m^{-1}.

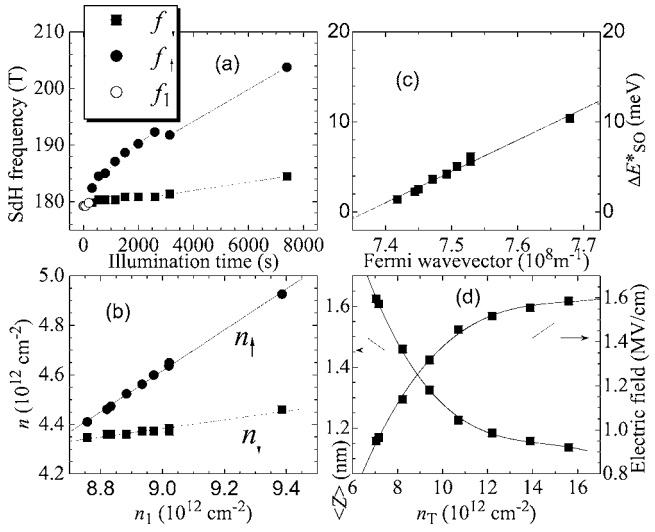

FIG. 4. (a) The SdH frequencies obtained from Fig. 3. (b) The carrier concentrations of spin-up ($n_\uparrow$) and spin-down ($n_\downarrow$) first subbands versus the total carrier concentration of the first subband ($n_1=n_\uparrow+n_\downarrow$). (c) The effective spin-splitting energy (ΔE^*_{SO}) versus the Fermi wave vector. (d) The calculated electric field ($\boldsymbol{E}$) and average distance of electron from the heterointerface $\langle z\rangle$ against the total sheet carrier concentration (n_T).

IV. DISCUSSIONS

The 2D Hamiltonian of Rashba and Dresselhaus terms can be written as $\boldsymbol{H}_{\mathrm{SO}}(\boldsymbol{k})=[\alpha_{wz}-\gamma_{wz}(b\langle k_z^2\rangle-k_\parallel^2)](\sigma_x k_y-\sigma_y k_x)$, and the effective spin-splitting energy becomes $\Delta E^*_{\mathrm{SO}}(k)=2[(\alpha_{wz}-\gamma_{wz}b\langle k_z^2\rangle)k_\parallel+\gamma_{wz}k_\parallel^3]$. It can be separated into linear-$k_\parallel$ and cubic-$k_\parallel$ terms. If $\boldsymbol{H}_{\mathrm{SO}}$ is solely governed by the Rashba term ($\gamma_{wz}=0$), a beating pattern of SdH oscillations arises from two isotropic spin-splitting concentric Fermi circles. However, if $[\alpha_{wz}-\gamma_{wz}(b\langle k_z^2\rangle-k_\parallel^2)]=0$, the two-spin subbands are degenerate (i.e., $\Delta E^*_{\mathrm{SO}}=0$), and hence, the beating pattern does not appear [e.g., twofold spin degenerate with a constant $\langle k_z\rangle$ in Fig. 1(a)]. As we mentioned before, the mechanism of spin splitting in $Al_xGa_{1-x}N/GaN$ consists of four parts: Rashba (α_{wz}) term, Dresselhaus (γ_{wz}) term, piezoelectric field, and Δ_{C1}-Δ_{C3} coupling. Garrido *et al.* showed that the electric field $\boldsymbol{E}$ due to the piezoelectric and spontaneous polarization depends linearly on Al composition.[24] The Rashba coefficient α_{wz} thus increases linearly with Al composition, $\alpha_{wz}(x)=\alpha_0 e\boldsymbol{E}+\boldsymbol{C}_{\mathrm{WSIA}}$. In the meanwhile, the stronger electric field gives a better quantum confinement (i.e., a smaller confinement size d). As a result, $\langle k_z^2\rangle$ increases with Al composition as well, and hence, the Fermi wave vector $\boldsymbol{k}^F=(k_\parallel^F,k_z^F)$ of 2DEG will be pushed toward the anticrossing zone of Δ_{C1} and Δ_{C3} bands.[22] The spin-splitting energy (mainly the Dresselhaus term) is tremendously enhanced by the Δ_{C1}-Δ_{C3} coupling due to the increased p-wave probability in the Δ_{C1} band, leading to an enhancement of the effective Dresselhaus constant (γ^*_{wz}). As long as the spin-degenerate equation is held, the $\Delta E^*_{\mathrm{SO}}(k)$ vanishes due to the interference of Rashba and Dresselhaus terms (i.e., no beating SdH oscillations). If the equation is broken with a variation of $k_\parallel^F$ (e.g., by the PPC effect here or by a gate voltage in Ref. 15), the beating pattern occurs [e.g., as observed in Fig. 2(a) and repeated in Fig. 3(a)]. Since both $k_\parallel^F$ and $\langle k_z^F\rangle$ are functions of the 2D carrier concentration, we define a characteristic wave vector: the threshold wave vector ($k_\parallel^{\mathrm{th}}$), at which the twofold degeneracy is just broken, leading to a nonvanishing $\Delta E^*_{\mathrm{SO}}(k)$. In Fig. 4(c), we fitted the $\Delta E^*_{\mathrm{SO}}(k)$ versus $(k_\parallel^F)^3$, the dotted line, and obtained the threshold wave vector $k_\parallel^{\mathrm{th}}=7.37\times10^8$ m^{-1}. We also fitted the $\Delta E^*_{\mathrm{SO}}(k)$ versus linear $k_\parallel^F$ for comparison (the solid line). It is found that these two fits do not have much difference in the measured $k_\parallel^F$. The threshold $k_\parallel^{\mathrm{th}}$ should be smaller than the value of $\langle k_z^F\rangle$. The size of quantum confinement can be written as $d=2\langle z\rangle$, where $\langle z\rangle$ is the average distance of electron from the heterointerface (see Fig. 5). We estimated the electric field $\boldsymbol{E}$ and the average distance $\langle z\rangle$ as functions of the total sheet carrier concentration n_T by a self-consistent solution of Poisson and Schrödinger equations. The material parameters for the piezoelectric coefficients in Ref. 24 were used. The results of calculated $\langle z\rangle$ and $\boldsymbol{E}$ are shown in Fig. 4(d). The $\langle z\rangle$ is about 1.40 nm at $n_T=8.65\times10^{12}$ cm^{-2} and reduces to 1.29 nm at $n_T=9.87\times10^{12}$ cm^{-2}, but the $\boldsymbol{E}$ increases from 1.22 to 1.36 MV/cm. Thus, the calculated $\langle k_z^F\rangle$ is 1.12×10^9 m^{-1}, which is greater than the threshold wave vector, as we predicted. The value of $\langle(k_z^F)^2\rangle$ increases by 18%, but the $\boldsymbol{E}$ increases only by 11%. Therefore, the degen-

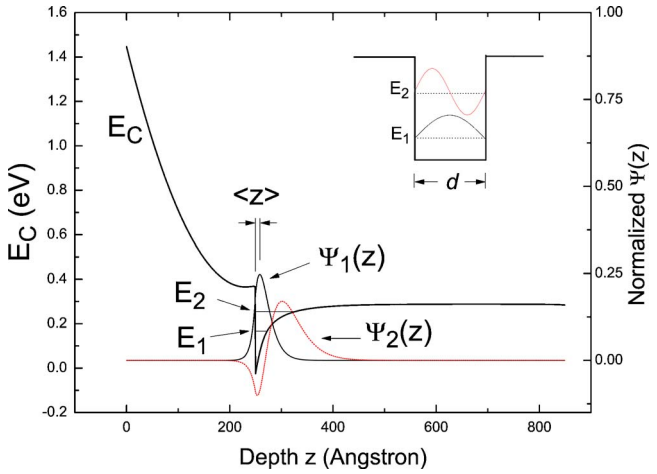

FIG. 5. (Color online) For a 2DEG in an ideal square QW (see the inset), the quantized wave vector k_z and the quantum confinement d is related to $k_z d=(i+1)\pi$. For the first subban $(i=0)$, $k_z=(\pi/d)$. The size of quantum confinement can be written as $d=2\langle z\rangle$, where $\langle z\rangle$ is the average distance from barrier, and hence, $k_z=\pi/2\langle z\rangle$. This k_z is independent of the Fermi level. However, for a 2DEG in a heterostructure, the quantum confinement, $d=2\langle z\rangle$, is no longer a constant due to the band bending at the heterojunction. The band bending is dependent on the carrier concentration and the sample parameters (e.g., x and Si-doping level). As a result, the quantized wave vector is dependent on the Fermi level, denoted as $\langle k_z^F\rangle$.

eracy of two spin subbands was broken, and hence, the Dresselhaus term starts to dominate $\Delta E_{\mathrm{SO}}^{*}(k)$. The nonvanishing $\Delta E_{\mathrm{SO}}^{*}(k)$ for beating pattern depends on the competition between Rashba (α_{wz}) and Dresselhaus (β_{wz}) terms, resulting in the varied $\Delta E_{\mathrm{SO}}^{*}(k)$ observed in $Al_xGa_{1-x}N/GaN$ (Table I). It is noted that the Si-doping level at $Al_xGa_{1-x}N$ will alter both $\boldsymbol{E}$ and $\langle z\rangle$, yielding a fluctuation in $\Delta E_{\mathrm{SO}}^{*}(k)$. Besides, the band gap in the $Al_xGa_{1-x}N$ layer is a function of Al composition with an effective bowing parameter of 0.8,[24] yielding an x-dependent band offset (the barrier height) and polarization-induced field discontinuity (e.g., the piezoelectric effect) at the heterointerface. The effective spin-splitting energy $\Delta E_{\mathrm{SO}}^{*}(k)$ is therefore x dependent as well. For instance, Garrido *et al.* calculated that the field discontinuity is about 0.9 MV/cm for $x=0.15$ and it increases by ~90% when Al composition is extrapolated to $x=0.3$.[24] The Rashba linear-$\boldsymbol{k}$ term $(\alpha_0 e\boldsymbol{E})$ is thus enhanced by ~90% when Al composition increases from $x=0.15$ to 0.3. In Ref. 17, Thillosen *et al.* observed the SdH beating pattern in $Al_xGa_{1-x}N/GaN$ for samples 1 and 2 (both $x=0.15$) but not observed for sample 3 $(x=0.3)$. They attributed the origin of the SdH beating pattern to the inhomogeneities and did not explain why no beating pattern is observed for sample 3. Our model presented here provides a possible explanation. The reason is that samples 1 and 2 in Ref. 17 have a smaller Rashba linear-$\boldsymbol{k}$ term due to a smaller polarization-induced field $(x=0.15)$, resulting in a nondegenerate spin-splitting state which gives rise to a beating pattern in SdH oscillations. On the contrary, for sample 3, its Rashba linear-$\boldsymbol{k}$ term becomes much greater (due to the stronger polarization-induced field for $x=0.3$ as compared to $x=0.15$). The interference of Rashba and Dresselhaus effects yields a spin-degenerate state, and hence, no beating pattern is observed in the SdH measurements.

V. CONCLUSION

We have observed the spin-splitting beat pattern in SdH oscillations. From the temperature-dependent SdH measurement, we eliminated the possibility of MIS for the beating pattern of SdH oscillations. We also ruled out the possibility of inhomogeneity effect due to the absence of negative magnetoresistance. We presented an evidence for the spin-degenerate state in $Al_xGa_{1-x}N/GaN$ due to the interference of Rashba and Dresselhaus effects. The nonvanishing $\Delta E_{\mathrm{SO}}^{*}(k)$ for the beating pattern of SdH oscillations depends on the competition between Rashba (α_{wz}) and Dresselhaus (β_{wz}) terms. The dominant mechanism for the k-dependent spin splitting at high values of k is attributed to the Dresselhaus term which is enhanced by the Δ_{C1}-Δ_{C3} coupling of the wurtzite band folding effect. The model for the interference of Rashba and Dresselhaus effects can explain the varied $\Delta E_{\mathrm{SO}}^{*}(k)$ observed in $Al_xGa_{1-x}N/GaN$ obtained by many groups. Based on the model, the effective spin-splitting energy $\Delta E_{\mathrm{SO}}^{*}(k)$ in the $Al_xGa_{1-x}N/GaN$ heterostructure is gate controllable for the spin-polarized field-effect transistor.

ACKNOWLEDGMENTS

This project is supported in part by National Research Council of Taiwan and NRC Core Facilities Laboratory for Nanoscience and Nanotechnology in Kaohsiung-Pingtung Area. The authors are grateful to S. Y. Liang, C. P. Yu, C. Z. Chang, and K. R. Wang for their assistance.

*Electronic mail: ikailo@mail.phys.nsysu.edu.tw

[1] *Semiconductor Spintronics and Quantum Computation*, edited by D. D. Awschalom, D. Loss, and N. Samarth (Springer, Berlin, 2002).

[2] I. Zutic, J. Fabian, and S. Das Sarma, Rev. Mod. Phys. **76**, 323 (2004).

[3] R. M. White, *Quantum Theory of Magnetism* (Springer-Verlag, Berlin, 1983), Chap. 2, p. 29.

[4] R. I. Rashba, Sov. Phys. Solid State **2**, 1109 (1960); Yu. A. Bychkov and E. I. Rashba, J. Phys. C **17**, 6039 (1984).

[5] G. Dresselhaus, Phys. Rev. **100**, 580 (1955).

[6] E. I. Rashba and V. I. Sheka, Sov. Phys. Solid State **3**, 1257 (1961).

[7] N. S. Averkiev, L. E. Golub, and M. Willander, J. Phys.: Condens. Matter **14**, R271 (2002).

[8] Al. L. Efros and E. I. Rashba, Phys. Rev. B **73**, 165325 (2006).

[9] S. D. Ganichev *et al.*, Phys. Rev. Lett. **92**, 256601 (2004).
[10] David Z.-Y. Ting and X. Cartoixa, Phys. Rev. B **68**, 235320 (2003).
[11] S. A. Tarasenko and N. S. Averkiev, JETP Lett. **75**, 552 (2002).
[12] J. Nitta, T. Akazaki, H. Takayanagi, and T. Enoki, Phys. Rev. Lett. **78**, 1335 (1997).
[13] For review, see W. Zawadzki and P. Pfeffer, Semicond. Sci. Technol. **19**, R1 (2004).
[14] I. Lo *et al.*, Phys. Rev. B **65**, 161306(R) (2002); I. Lo, W. T. Wang, M. H. Gau, J. K. Tsai, S. F. Tsay, and J. C. Chiang, Appl. Phys. Lett. **88**, 082108 (2006).
[15] K. Tsubaki *et al.*, Appl. Phys. Lett. **80**, 3126 (2002).
[16] K. S. Cho *et al.*, Appl. Phys. Lett. **86**, 222102 (2005).
[17] N. Thillosen, S. Cabanas, N. Kaluza, V. A. Guzenko, H. Hardtdegen, and T. Schapers, Phys. Rev. B **73**, 241311(R) (2006).
[18] N. Tang *et al.*, Appl. Phys. Lett. **88**, 172112 (2006).
[19] S. L. Chuang and C. S. Chang, Phys. Rev. B **54**, 2491 (1996); V. I. Litvinov, *ibid.* **68**, 155314 (2003).
[20] L. C. LewYan Voon, M. Willatzen, M. Cardona, and N. E. Christensen, Phys. Rev. B **53**, 10703 (1996); L. C. Lew Yan Voon *et al.*, Appl. Phys. Lett. **87**, 041906 (2005).
[21] G. Dresselhaus, Phys. Rev. **105**, 135 (1957); G. Dresselhaus, J. Phys. Chem. Solids **1**, 14 (1956).
[22] I. Lo, W. T. Wang, M. H. Gau, S. F. Tsay, and J. C. Chiang, Phys. Rev. B **72**, 245329 (2005).
[23] W. Weber *et al.*, Appl. Phys. Lett. **87**, 262106 (2005); S. Schmult, M. J. Manfra, A. Punnoose, A. M. Sergent, K. W. Baldwin, and R. J. Molnar, Phys. Rev. B **74**, 033302 (2006).
[24] J. A. Garrido *et al.*, Appl. Phys. Lett. **75**, 2407 (1999).
[25] A. Y. Polyakov *et al.*, Appl. Phys. Lett. **83**, 3314 (2003).
[26] I. Lo *et al.*, Phys. Rev. B **74**, 245325 (2006).
[27] K. S. Cho *et al.*, J. Appl. Phys. **96**, 7370 (2004).
[28] E. A. de Andrada e Silva, G. C. La Rocca, and F. Bassani, Phys. Rev. B **50**, 8523 (1994).
[29] N. S. Averkiev, M. M. Glazov, and S. A. Tarasenko, Solid State Commun. **133**, 543 (2005).
[30] I. Lo, S. J. Chen, L. W. Tu, W. C. Mitchel, R. C. Tu, and Y. K. Su, Phys. Rev. B **60**, R11281 (1999).